Structure and Mechanism of an Amino Acid Antiporter

Xiang Gao,[1,2]* Feiran Lu,[1,2]* Lijun Zhou,[1,2]* Shangyu Dang,[1,2] Linfeng Sun,[1,2] Xiaochun Li,[1,2] Jiawei Wang,[1,2] Yigong Shi[2,3]†

Virulent enteric pathogens such as *Escherichia coli* strain O157:H7 rely on acid-resistance (AR) systems to survive the acidic environment in the stomach. A major component of AR is an arginine-dependent arginine:agmatine antiporter that expels intracellular protons. Here, we report the crystal structure of AdiC, the arginine:agmatine antiporter from *E. coli* O157:H7 and a member of the amino acid/polyamine/organocation (APC) superfamily of transporters at 3.6 Å resolution. The overall fold is similar to that of several Na^+-coupled symporters. AdiC contains 12 transmembrane segments, forms a homodimer, and exists in an outward-facing, open conformation in the crystals. A conserved, acidic pocket opens to the periplasm. Structural and biochemical analysis reveals the essential ligand-binding residues, defines the transport route, and suggests a conserved mechanism for the antiporter activity.

Enteric bacteria, including *Shigella*, *Salmonella*, *Yersinia*, and *Escherichia coli* strain O157:H7, are among the most virulent pathogens (*1*). To survive the extremely acidic environment (pH 2 to 3) of the stomach, these bacteria have acquired elaborate systems to maintain a higher intracellular pH (*2*). In *E. coli*, the acid-resistance systems 2 (AR2) and 3 (AR3) expel intracellular protons through two coupled processes: intracellular decarboxylation of glutamate (Glu) and arginine (Arg) by AR2 and AR3, respectively, and the exchange of the reaction products, γ-aminobutyric acid (GABA) and agmatine (Agm), with extracellular Glu and Arg (*2*). The Glu:GABA antiporter GadC (*3*, *4*) and the Arg:Agm antiporter AdiC (*5*, *6*) are at the center of the systems.

AdiC and GadC are members of the amino acid/polyamine/organocation (APC) superfamily [transporter class (TC) no. 2.A.3] of membrane transporters, which has at least 250 members in diverse organisms (*7*, *8*). AdiC shares considerable sequence similarity with GadC; the lysine:cadaverine antiporter, CadB (*9*, *10*); and the ornithine:putrescine antiporter, PotE (*11*–*13*). AdiC couples the influx of Arg with the efflux of Agm, resulting in net expulsion of one proton for each transport cycle (*5*, *14*). Recombinant AdiC is a homodimer in both detergent micelles and lipid mem-

[1]State Key Laboratory of Bio-membrane and Membrane Biotechnology, Tsinghua University, Beijing 100084, China. [2]Center for Structural Biology, Department of Biological Sciences and Biotechnology, Tsinghua University, Beijing 100084, China. [3]School of Medicine, Tsinghua University, Beijing 100084, China.

*These authors contributed equally to this work.
†To whom correspondence should be addressed. E-mail: shi-lab@tsinghua.edu.cn

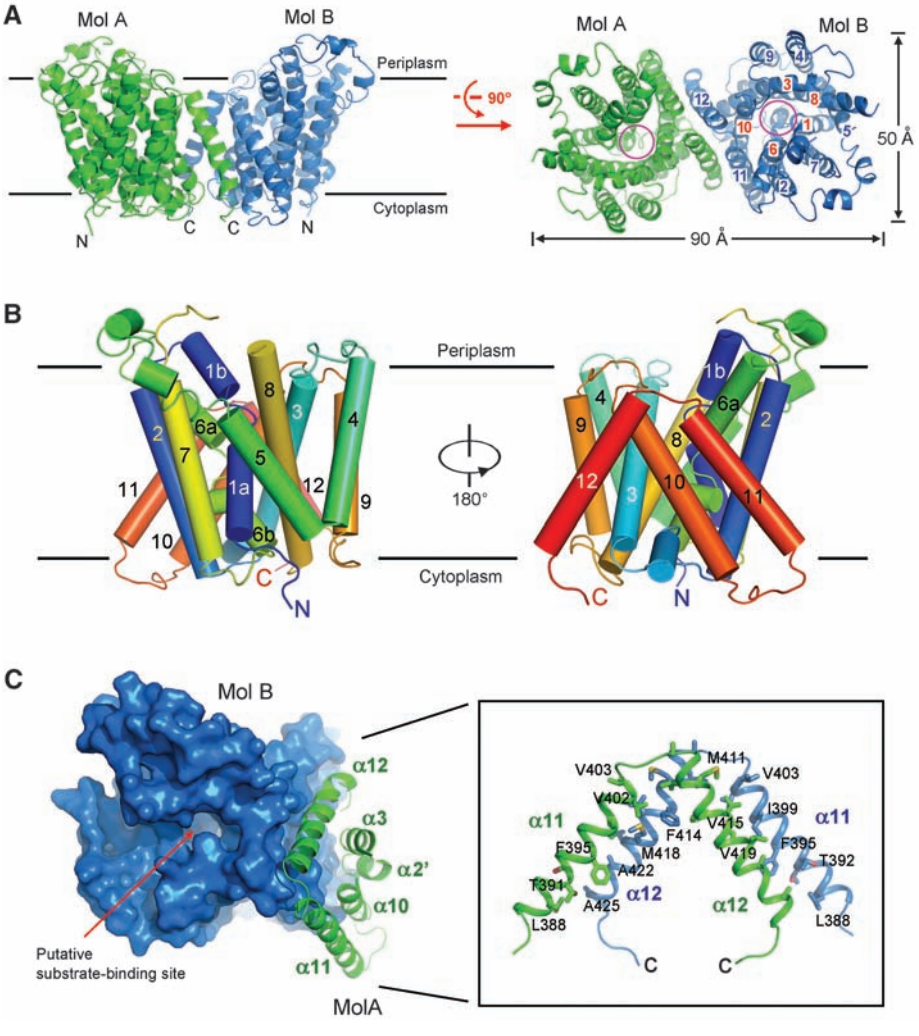

Fig. 1. Structure of AdiC, an amino acid antiporter of the APC superfamily. (**A**) Structure of the AdiC homodimer in an asymmetric unit in the $P2_12_12_1$ space group. Two perpendicular views are shown. Each molecule of AdiC consists of an inner layer of five TMs (red labels) and an outer layer of seven TMs (blue labels). The magenta circles indicate the location of the central cavity in AdiC. (**B**) A close-up view of an AdiC protomer. Note that TM1 and TM6 each consists of two α-helical segments that are connected by short, conserved sequence loops. (**C**) Dimerization interface of AdiC. Homodimerization is mediated mainly by TM11 and TM12. Specific amino acids that contribute to homodimerization are labeled in the right-hand image (*30*). The central cavity is thought to be the substrate-binding site. [Figures 1 to 3 were prepared with use of PyMol (*31*)]

branes and facilitates Arg:Agm exchange between pH 4 and 8 (*8*, *15*). The available structural information on the APC superfamily is limited to low-resolution structures of AdiC (*8*) and another protein (*16*), which were derived from electron crystallography and electron microscopy, respectively.

We purified recombinant AdiC as described (*15*, *17*). After screening more than 800 crystals in several space groups, we achieved a diffraction limit of 3.6 Å resolution for crystals grown in the $P2_12_12_1$ space group. The structure was determined by osmium-based, single-wavelength anomalous dispersion (SAD) (table S1 and fig. S1). Sequence assignment was facilitated by difference Fourier analysis of SeMet-labeled (where Met indicates methionine) protein (fig. S2). Each asymmetric unit contains two molecules of AdiC, which form a homodimer, with a pseudo-twofold symmetry axis perpendicular to the lipid membrane (Fig. 1A). We also solved the structure of AdiC in the *P*1 space group, which contains four molecules in an asymmetric unit (table S1 and fig. S3). These four molecules are organized into two homodimers, each with the same structure as that in the $P2_12_12_1$ space group (fig. S3). For simplicity, we only discuss one AdiC homodimer.

Despite lack of sequence similarity, AdiC exhibits the same fold as that of the Na^+-coupled symporters, including $LeuT_{Aa}$ of the neurotransmitter sodium symporter (NSS) family (*18*), BetP of the betaine/chlorine/carnitine transporters (BCCT) family (*19*), vSGLT of the sodium solute symporter (SSS) family (*20*), and Mhp1 of the nucleobase-cation-symport-1 (NCS1) family (*21*). This finding confirms an earlier prediction (*22*). Each molecule of AdiC has 12 transmembrane segments (TMs), arranged in two layers (Fig. 1 and fig. S4). The inner layer, containing TM1, TM3, TM6, TM8, and TM10, is surrounded by the outer layer, consisting of TM2, TM4, TM5, TM7, TM9, TM11, and TM12 (Fig. 1, A and B). Similar to the Na^+-coupled symporters (*18*–*21*), TM1 to TM5 are structurally related to TM6 to TM10 (fig. S5), with a root mean square deviation of 3.7 Å over 116 Cα atoms. Each AdiC molecule contains a centrally located cavity, which opens to the periplasmic side (Fig. 1, A and C).

As in the Na^+-coupled symporters (*18*–*21*), TM1 and TM6 are disrupted by short, nonhelical, Gly-containing loops (Fig. 1B). Amino acids in these loops are highly conserved within distinct families of the APC superfamily. For example, AdiC, CadB, and PotE, which all belong to the basic amino acid:polyamine antiporter (APA) family (*7*), share two signature loop sequences, the GSG motif (Gly^{25}-Ser^{26}-Gly^{27}) in TM1 and the GVESA motif (Gly^{206}-Val-Glu-Ser-Ala^{210}) in TM6 (fig. S4). The discontinuity of transmembrane helices has also been observed in other classes of transporters (*23*), including the Ca^{2+}–adenosine triphosphatase (ATPase) (*24*), the H^+/Cl^- exchanger CLC (*25*), the Na^+/H^+ exchanger NhaA (*26*), and the glutamate and aspartate transporter Glt_{Ph} (*27*, *28*). The unwound helices expose ordered carbonyl and amide groups, which may facilitate interactions with the substrate (*23*) and aid conformational switches required for substrate transport (*29*).

The homodimeric interface of AdiC involves four TMs from each molecule. Hydrophobic amino acids from TM11 of one AdiC molecule interdigitate with nonpolar residues from TM12 of the adjacent molecule (Fig. 1C). Additional interactions are mediated by the N-terminal portion of TM3 and the C-terminal portion of TM10. Comparison with the Na^+-coupled symporters (*18*–*21*) suggests that dimerization mediated by TM11 and TM12 may be unique to the APC superfamily.

Among TMs of the inner layer, TM6 appears to exhibit the largest degree of conformational difference among AdiC and the four Na^+-coupled symporters (fig. S6). The N-terminal backbone of TM6 in AdiC is shifted by 5, 9, and 14 Å, respectively, relative to the corresponding structural elements in $LeuT_{Aa}$, BetP, and vSGLT. TM10 also displays marked conformational variations among these transporters (fig. S6). This analysis suggests that TM6 and TM10 might play an important role in the transport process. Supporting this analysis, TM6 contributes to substrate binding in all four Na^+-coupled symporters (*18*–*21*), and TM10 was proposed to control substrate access to the periplasm (*21*).

Amino acids that are invariant among AdiC, CadB, and PotE, three APA family antiporters (*7*), were mapped onto the structure of AdiC (Fig. 2A). About a third of the conserved, polar or charged amino acids are clustered in the central cavity and its vicinity, making the central cavity the most conserved area in the entire molecule (Fig. 2B) and suggesting that it may be the substrate-binding site. The central cavity measures about 20 Å in depth and 5 to 10 Å in diameter. The bottom of the cavity is defined by four polar or charged amino acids: Asn^{22} at the C-terminal end of TM1a, Tyr^{93} in the middle of TM3, Glu^{208} at the breakage point of TM6, and Tyr^{365} in the middle of TM10 (Fig. 2B). The surface of the

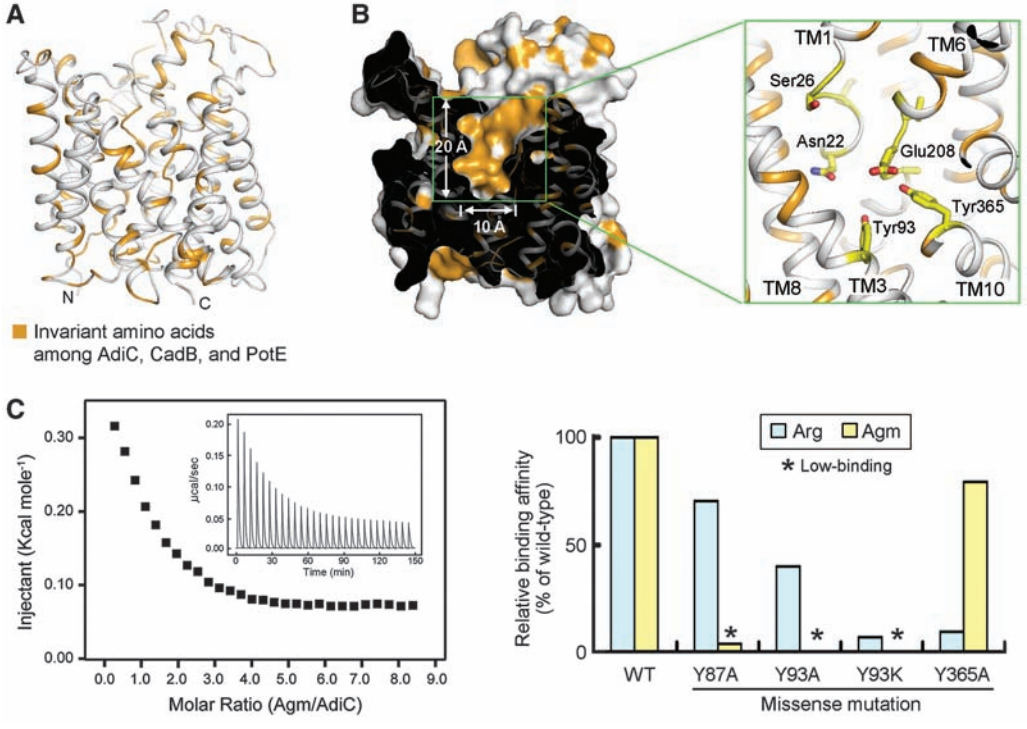

Fig. 2. Identification and features of the substrate-binding site. (**A**) Mapping conserved amino acids onto the structure of AdiC. Amino acids that are invariant among AdiC, CadB, and PotE are colored orange. (**B**) Identification of a putative substrate-binding site. The central cavity of AdiC is enriched with conserved amino acids, opens to the periplasm, and is likely the binding site for substrate (left). A close-up view shows a number of polar and charged amino acids, including Asn^{22} and Ser^{26} from TM1, Tyr^{93} from TM3, Glu^{208} from TM6, and Tyr^{365} from TM10. (**C**) Substrate binding by AdiC as measured by ITC. (Left) A representative ITC experiment, in which Agm was titrated into a solution of AdiC. (Inset) The original titration traces. (Right) The relative binding affinities for four AdiC mutants (*30*) compared with that of the WT protein. The association constant for the WT protein was standardized as 100%. Asterisks indicate three cases of low-affinity binding for Agm, where, despite readily detectable binding, curve fitting was difficult.

cavity is lined by a number of invariant residues, including the GSG motif from TM1; Tyr[87] and Tyr[101] from TM3; Val[217], Asn[219], and the GVESA motif from TM6; Cys[286], Ser[289], Leu[290], and Trp[293] from TM8; and Val[358] from TM10 (fig. S4). The negative electrostatic potential of the central cavity may contribute to binding of the positively charged substrate molecules such as Arg and Agm (fig. S7).

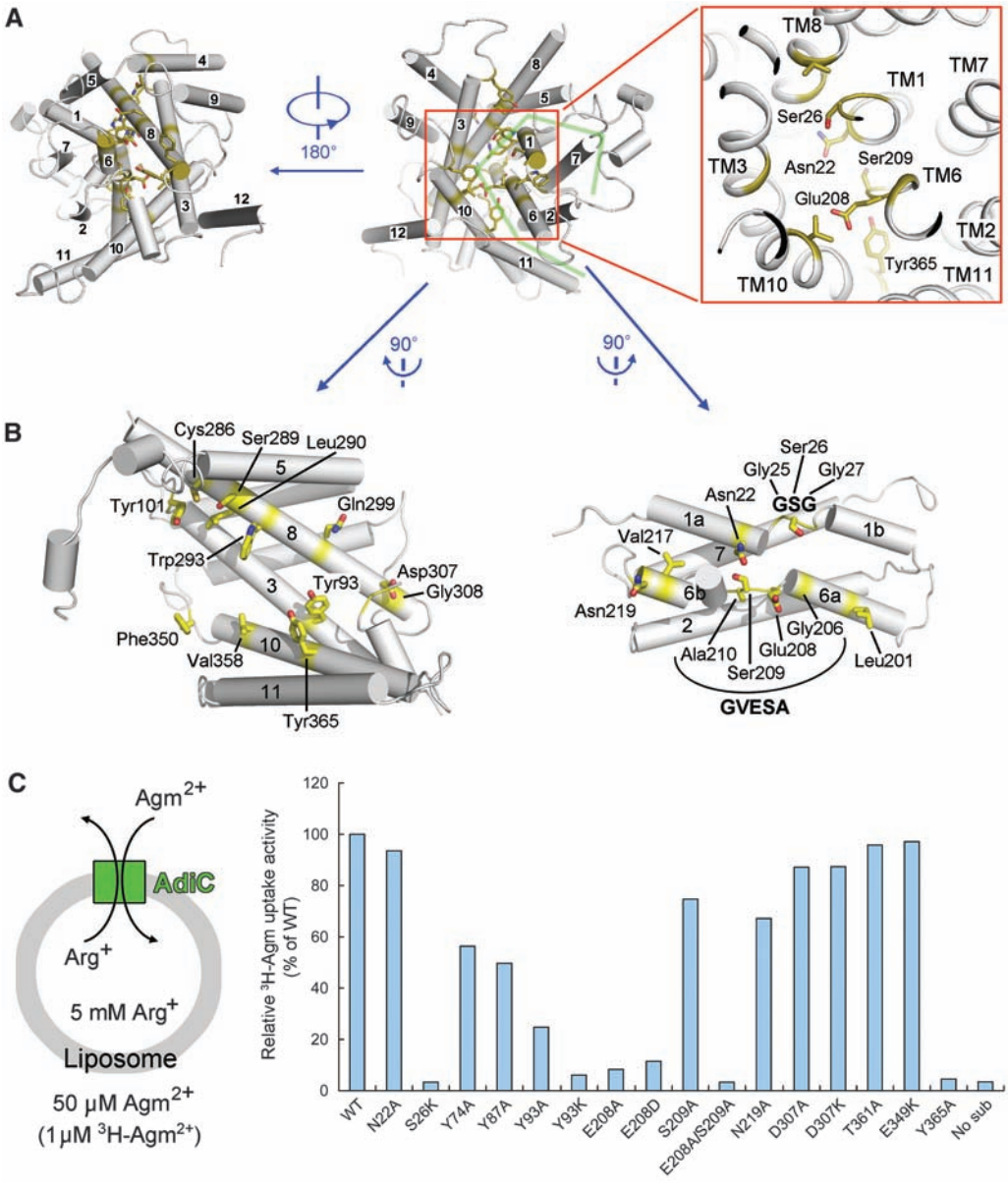

Fig. 3. Identification and features of the transport route. (**A**) Substrate transport route along the central axis. The putative transport route is identified by residues (colored yellow) that are invariant among AdiC, CadB, and PotE. The cytoplasmic and periplasmic sides of the route are depicted in the left and middle images, respectively. The right image highlights a few key residues. (**B**) Composition of the amino acids along the transport route. The structure of AdiC is separated into two portions to show all 25 highly conserved amino acids along the transport route, of which 60% are polar or charged. (**C**) Characterization of the antiport activity for WT and mutant AdiC. The left image depicts the assay. Uptake of ^{3}H-labeled Agm into the AdiC-incorporated liposome was monitored. The right graph summarizes the result. The values shown represent the average of three independent experiments. The standard deviations were estimated to be 10 to 15% of the values shown.

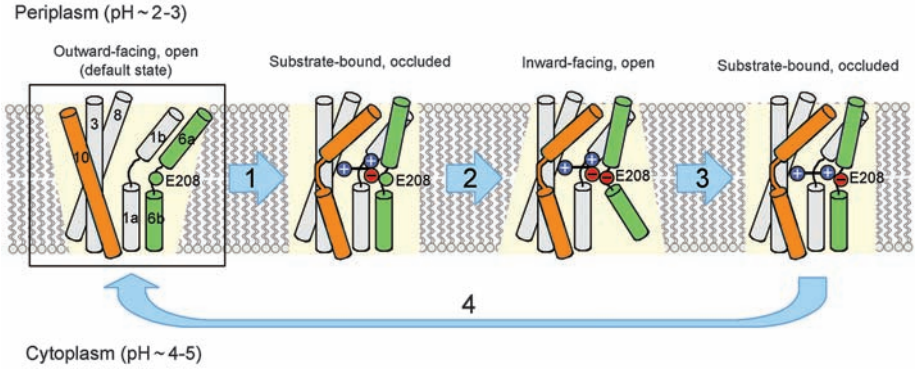

Fig. 4. A working model for AdiC and the APA family of antiporters. The antiport activity of AdiC may involve four sequential steps. The default state is likely to be the current structure, in an open, outward-facing conformation. Step 1, substrate binding to the antiporter results in occlusion of primary substrate to the periplasm. Step 2, the antiporter switches to an open, inward-facing conformation, where Arg is competitively displaced by Agm. Step 3, the antiporter bound to the secondary substrate closes down and occludes the substrate from the cytoplasm. Step 4, the antiporter opens up to the periplasm, allowing the release of the secondary substrate, completing the antiport cycle. Under extremely acidic conditions such as the stomach, Glu[208] is proposed to be the sensor amino acid in AdiC, which remains protonated at periplasmic pH but undergoes deprotonation at cytoplasmic pH. Differences in protonation states are proposed to contribute to differential binding of primary and secondary substrates. TM6 and TM10 are thought to undergo conformational changes in response to substrate binding.

To characterize the role of the conserved amino acids, we generated a number of missense mutations and evaluated their impacts on substrate binding by using isothermal titration calorimetry (ITC). As previously reported (*8*, *15*), substrate binding by AdiC is endothermic (Fig. 2C, left). The association constant (K_a) was estimated by curve fitting, and AdiC interacts with Agm with a K_a value that is about eight times higher than that for Arg (*8*, *15*). To facilitate comparison, we represented K_a values of the mutant proteins as a percentage of that for the wild-type (WT) AdiC (Fig. 2C, right). The mutation Y93K (*30*), at the bottom of the cavity, nearly crippled binding to both Arg and Agm. Y87A, on the cytoplasmic side, markedly reduced binding affinity for Agm but not for Arg. This observation is consistent with the antiporter function of AdiC: transporting Arg into, while expelling Agm out of, the cytoplasm. In contrast, Y365A, at the bottom of the cavity, markedly weakened binding to Arg but not to Agm (Fig. 2C). This analysis confirms the central cavity as the substrate-binding site and identifies key residues that are involved in binding to Arg and Agm. The observation that binding to Arg and Agm was simultaneously affected by mutations of Tyr^{93} suggests that the binding site for Arg may at least partially overlap with that for Agm.

A number of conserved, polar amino acids are located below the substrate-binding cavity and along the central axis (Fig. 3, A and B), which likely constitute the route of transport. We generated a number of missense mutations in the putative transport route and evaluated their impacts on the antiporter activity of AdiC by monitoring the uptake of ^{3}H-labeled Agm in an in vitro proteoliposome-based transport assay (*8*, *15*) (Fig. 3C, left). In the absence of substrate (Arg) in the liposome, the uptake of ^{3}H-labeled Agm was at background level (Fig. 3C, right). The WT AdiC showed robust antiport activity, with a transport rate of about 60 μmoles per mg of AdiC within the first 5 min. This transport rate is very similar to that reported previously (*15*). Four mutations, S26K, Y93K, E208A, and Y365A (*30*), which affect amino acids at the bottom of the substrate-binding site, led to abrogation of antiport activity (Fig. 3C). Consistent with this finding, Y93K exhibited crippled binding to Arg and Agm, and Y365A had markedly reduced binding affinity for Arg (Fig. 3D). Y87A and Y93A, each exhibiting severely compromised binding to Agm and weakened binding to Arg (Fig. 2C), also displayed reduced levels of antiporter activity (Fig. 3C). By contrast, a number of other mutations had little impact on the uptake of ^{3}H-labeled Agm. This analysis identifies amino acids that directly contribute to the antiport activity.

The antiport activity of AdiC may involve four sequential steps. The default state is likely to be the current structure, in an open, outward-facing conformation (Fig. 4). First, substrate binding leads to the occlusion of the bound, primary substrate (Arg) to the periplasm. Second, the antiporter switches to an open, inward-facing conformation, where Arg is competitively displaced by Agm, the secondary substrate. Third, the antiporter bound to the secondary substrate closes down and occludes the bound substrate from the cytoplasm. In the fourth and final step, the antiporter opens up to the periplasm, releasing the secondary substrate. Although the general folds of AdiC and the Na^+-coupled symporters are similar, their modes of substrate binding markedly deviate from each other (fig. S8). The conformation of the TMs surrounding the putative substrate-binding site in AdiC closely resembles that of $LeuT_{Aa}$. It remains to be seen how AdiC interacts with substrate molecules and carries out its antiport activity.

On the basis of our structural and biochemical analysis, we propose that Glu^{208}, invariant among AdiC, CadB, and PotE (fig. S4), is a pH sensor and plays a major role in the antiport activity. In the stomach (pH 2 to 3), Glu^{208}, with $pK_a \sim 4.25$, is predominantly protonated. The majority of the extracellular substrate amino acids are deprotonated in their α-carboxylate groups ($pK_a \sim 2$). Thus, the majority of these amino acids carry no net charge on their head groups, with the positively charged α-amino group offsetting the negatively charged α-carboxyl group. Protonated Glu^{208} likely binds to the neutral head groups of the substrate amino acid (Fig. 4). Once facing the intracellular environment (pH 4 to 5), the sensor residue Glu^{208} is likely to deprotonate, thus developing a net negative charge in the substrate-binding cavity. The negative charge may favor binding by the positively charged head group of the α-decarboxylated amino acid (Fig. 4). Consequently, the secondary substrate (Agm) displaces the primary substrate (Arg) on the antiporter.

What structural elements undergo the proposed conformational changes during transport? Gouaux and colleagues proposed that TM1 and TM6 might be the toggle switches (*18*). This model gained additional support from a recent structural study on BetP (*19*). By contrast, Weyand *et al*. argued that TM3 and TM8 may adopt alternating conformations to allow the switches from outward-open to inward-open (*21*). These conjectures have their bases mostly in structural comparison of different molecules in different transport states: $LeuT_{Aa}$ (*18*) and Mhp1 (*21*) in outward-facing states, vSGLT in inward-facing conformation (*20*), and BetP in between (*19*). The backbone of TM1 in AdiC appears to maintain a very similar conformation compared to that of the Na^+-coupled symporters (fig. S6). In contrast, TM6, and to a lesser extent, TM10, exhibit pronounced conformational shifts. Hence, we propose that TM6 may serve as the primary switch to allow different substrate-binding states and TM10 may facilitate the occlusion of substrate (Fig. 4).

References and Notes

1. M. S. Donnenberg, *Nature* **406**, 768 (2000).
2. J. W. Foster, *Nat. Rev. Microbiol.* **2**, 898 (2004).
3. B. M. Hersh, F. T. Farooq, D. N. Barstad, D. L. Blankenhorn, J. L. Slonczewski, *J. Bacteriol.* **178**, 3978 (1996).
4. M. P. Castanie-Cornet, T. A. Penfound, D. Smith, J. F. Elliott, J. W. Foster, *J. Bacteriol.* **181**, 3525 (1999).
5. R. Iyer, C. Williams, C. Miller, *J. Bacteriol.* **185**, 6556 (2003).
6. S. Gong, H. Richard, J. W. Foster, *J. Bacteriol.* **185**, 4402 (2003).
7. D. L. Jack, I. T. Paulsen, M. H. Saier, *Microbiology* **146**, 1797 (2000).
8. F. Casagrande *et al*., *J. Biol. Chem.* **283**, 33240 (2008).
9. W. Soksawatmaekhin, A. Kuraishi, K. Sakata, K. Kashiwagi, K. Igarashi, *Mol. Microbiol.* **51**, 1401 (2004).
10. W. Soksawatmaekhin, T. Uemura, N. Fukiwake, K. Kashiwagi, K. Igarashi, *J. Biol. Chem.* **281**, 29213 (2006).
11. K. Kashiwagi *et al*., *J. Biol. Chem.* **275**, 36007 (2000).
12. K. Kashiwagi, S. Miyamoto, F. Suzuki, H. Kobayashi, K. Igarashi, *Proc. Natl. Acad. Sci. U.S.A.* **89**, 4529 (1992).
13. K. Kashiwagi, S. Shibuya, H. Tomitori, A. Kuraishi, K. Igarashi, *J. Biol. Chem.* **272**, 6318 (1997).
14. A. Accardi, C. Miller, *Nature* **427**, 803 (2004).
15. Y. Fang, L. Kolmakova-Partensky, C. Miller, *J. Biol. Chem.* **282**, 176 (2007).
16. N. Reig *et al*., *J. Biol. Chem.* **282**, 13270 (2007).
17. Materials and methods are available as supporting material on *Science* Online.
18. A. Yamashita, S. K. Singh, T. Kawate, Y. Jin, E. Gouaux, *Nature* **437**, 215 (2005).
19. S. Ressl, A. C. Terwisscha van Scheltinga, C. Vonrhein, V. Ott, C. Ziegler, *Nature* **458**, 47 (2009).
20. S. Faham *et al*., *Science* **321**, 810 (2008).
21. S. Weyand *et al*., *Science* **322**, 709 (2008).
22. J. S. Lolkema, D. J. Slotboom, *Mol. Membr. Biol.* **25**, 567 (2008).
23. E. Screpanti, C. Hunte, *J. Struct. Biol.* **159**, 261 (2007).
24. C. Toyoshima, M. Nakasako, H. Nomura, H. Ogawa, *Nature* **405**, 647 (2000).
25. R. Dutzler, E. B. Campbell, M. Cadene, B. T. Chait, R. MacKinnon, *Nature* **415**, 287 (2002).
26. C. Hunte *et al*., *Nature* **435**, 1197 (2005).
27. D. Yernool, O. Boudker, Y. Jin, E. Gouaux, *Nature* **431**, 811 (2004).
28. O. Boudker, R. M. Ryan, D. Yernool, K. Shimamoto, E. Gouaux, *Nature* **445**, 387 (2007).
29. O. Jardetzky, *Nature* **211**, 969 (1966).
30. Single-letter abbreviations for the amino acid residues are as follows: A, Ala; C, Cys; D, Asp; E, Glu; F, Phe; G, Gly; H, His; I, Ile; K, Lys; L, Leu; M, Met; N, Asn; P, Pro; Q, Gln; R, Arg; S, Ser; T, Thr; V, Val; W, Trp; and Y, Tyr.
31. W. L. DeLano, www.pymol.org (2002).

32. We thank N. Shimizu at the Spring-8 beamline BL41XU and T. Kumasaka and S. Baba at beamline BL38XU for on-site assistance, Q. Liu for screening crystals at MacCHESS (Macromolecular Diffraction at the Cornell High Energy Synchrotron Source), and N. Yan for discussion and comments on the manuscript. This work was supported by funds from the Ministry of Science and Technology (grant no. 2009CB918801), Tsinghua University 985 Phase II funds, National Natural Science Foundation, and Beijing Municipal Commissions of Education and Science and Technology. The atomic coordinates have been deposited in the Protein Data Bank with the accession codes 3H5M and 3H6B.

Supporting Online Material

www.sciencemag.org/cgi/content/full/1173654/DC1
Materials and Methods
Figs. S1 to S8
Tables S1
References

17 March 2009; accepted 30 April 2009
Published online 28 May 2009;
10.1126/science.1173654
Include this information when citing this paper.

Structure and Mechanism of an Amino Acid Antiporter

Xiang Gao *et al.*

Science **324**, 1565 (2009);
DOI: 10.1126/science.1173654